Biogeosciences, 21, 2795–2809, 2024
https://doi.org/10.5194/bg-21-2795-2024
© Author(s) 2024. This work is distributed under
the Creative Commons Attribution 4.0 License.

Biogeosciences Open Access EGU



# The optimum fire window: applying the fire–productivity hypothesis to Jurassic climate states

**Teuntje P. Hollaar[1,2], Claire M. Belcher[1], Micha Ruhl[3], Jean-François Deconinck[4], and Stephen P. Hesselbo[2,5]**

[1]WildFIRE Lab, Global Systems Institute, University of Exeter, Exeter, EX4 4PS, UK
[2]Camborne School of Mines, Department of Earth and Environmental Sciences, University of Exeter, Penryn Campus, Penryn, TR10 9FE, UK
[3]Department of Geology, Trinity College Dublin, the University of Dublin, College Green, Dublin, Ireland
[4]Biogéosciences, UMR 6282 CNRS, Université de Bourgogne/Franche-Comté, 21000 Dijon, France
[5]Environment and Sustainability Institute, University of Exeter, Penryn Campus, Penryn, TR10 9FE, UK

**Correspondence:** Teuntje P. Hollaar (t.p.hollaar@uu.nl)

Received: 5 October 2023 – Discussion started: 10 October 2023
Revised: 26 March 2024 – Accepted: 27 March 2024 – Published: 13 June 2024

**Abstract.** Present-day fire frequency is related to a productivity–aridity gradient on regional and global scales. Optimum fire conditions occur at times of intermediate productivity and aridity, whereas fire is limited at the high productivity (moisture) and aridity (no fuel) endmembers. However, the current global fire activity pattern is reinforced by the predominant burning of grasslands. Here we test the intermediate fire–productivity hypothesis for a period on Earth before the evolution of grasses, the Early Jurassic, and explore the fire regime of two contrasting climatic states: the cooling of the Late Pliensbachian Event (LPE) and the warming of the Sinemurian–Pliensbachian Boundary (SPB). Palaeo-fire records are reconstructed from fossil charcoal abundance, and changes in the hydrological cycle are tracked via clay mineralogy, which allows inference of changes in fuel moisture status. Large fluctuations in the fossil charcoal on an eccentricity timescale indicate two modes of fire regime at the time. Wildfires were moisture-limited in a high-productivity ecosystem during eccentricity minima for both the SPB and the LPE. During eccentricity maxima fires increased, and an optimum fire window was reached, in which periodically greater seasonality in rainfall and temperatures led to intermediate states of productivity and aridity. The LPE experienced more extreme climatic endmembers compared to the SPB, with the fire regime edging closer to "moisture limitation" during eccentricity minima, and experienced more pronounced seasonality during eccentricity maxima, explained by the overall cooler climate at the time. This study illustrates that the intermediate-productivity gradient holds up during two contrasting climatic states in the Jurassic.

## 1 Introduction

The global distribution of fire at the present day follows the intermediate-productivity hypothesis. This hypothesis suggests that fire activity increases non-linearly along a productivity gradient primarily controlled by biomass and fuel availability (Pausas and Bradstock, 2007; Pausas and Ribeiro, 2013). Climate drives fuel availability, structure, and moisture, which are the main determinants of the fire regime. The fire regime reflects the frequency, behaviour, type of fire, and impact on the ecosystem (Bradstock, 2010). Fire is limited either by high moisture in ecosystems with high biomass production, for example in tropical rainforests, or by high aridity and low biomass production ecosystems with disconnected fuel, such as deserts. This principle explains drought-driven fire regimes and fuel-limited fire regimes (Pausas and Ribeiro, 2013). In humid regions, fires are initiated by seasonal aridity that leads to lower fuel moisture status and flammable conditions. Rising temperatures can lead to increased drought and flammability in high-productivity ecosystems and further accelerate this drought-driven increase in fire activity (Pausas and Ribeiro, 2013). In unproductive arid regions, it is biomass production that determines

fire activity as the fuel moisture status would not be limiting (Pausas and Ribeiro, 2013). The optimum window for wildfires is at intermediate-productivity levels, such as in the tropical savannahs of today wherein biomass can accumulate due to seasonal precipitation, and fuel becomes available in the dry season when the fuel moisture status decreases (Meyn et al., 2007; Pausas and Bradstock, 2007; Krawchuk and Moritz, 2011; Pausas and Paula, 2012; Pausas and Ribeiro, 2013).

The intermediate-productivity concept provides an effective explanation for the distribution of fire on a global and regional scale in the modern day, where the highest fire activity is found at intermediate moisture availability (Meyn et al., 2007; Krawchuk and Moritz, 2011; Daniau et al., 2012). The observation of high fire activity in ecosystems that are of intermediate aridity and productivity is strongly driven by grass biomes today (Archibald et al., 2018), where $> 80\,\%$ of the burnt area is in grasslands (van der Werf et al., 2006). Although the intermediate-productivity-gradient hypothesis of the present day is strongly linked to the expanse of grassland habitats, it should not require the presence of grasses to explain the impact of climate and seasonality on fire frequency in other vegetation types. The crucial concept is that an optimum fire window exists when there is a sufficiently moist season that allows fuel growth followed by a drier season in which fuel moisture levels are lowered, allowing for ignition and fire spread. Since fire has formed an important part of ecosystems and the Earth system since 420 Ma (Glasspool et al., 2004; Glasspool and Gastaldo, 2022), we therefore test whether the intermediate-productivity gradient has also existed since then and whether the concept can also be applied in a world before the evolution of grasses.

Here we look back at two contrasting climate events in the Early Jurassic, $\sim 190$ Myr ago, to assess what evidence there is for the existence of the intermediate-productivity fire gradient at such a time (Fig. 1). The first event, the Sinemurian–Pliensbachian Boundary event (SPB) is marked by global warming, sea-level rise, increased humidity, and a negative carbon-isotope excursion (Ruhl et al., 2016; Haq, 2018; Deconinck et al., 2019; Storm et al., 2020). In contrast, the second event, the Late Pliensbachian Event (LPE) is marked by $\sim 5\,^{\circ}$C cooling in northwestern Europe, greater aridity, sea-level fall, and a global positive carbon-isotope excursion (e.g. Korte et al., 2015; Ruhl et al., 2016; Haq, 2018; Deconinck et al., 2019; Storm et al., 2020). We couple charcoal, clay, and climate data to infer palaeo-fire and the hydrological regimes during both these time intervals.

## 2 Materials and methods

### 2.1 Materials

#### 2.1.1 Core samples

The records from both the LPE and the SPB are taken from the Llanbedr (Mochras Farm) borehole, from sedimentary strata deposited in a relatively deep marine setting close to the shore in the Cardigan Bay basin (Wales, UK). These sediments show a strong regular orbital control in the limestone–mudstone alternations (Ruhl et al., 2016), and an existing astrochronological framework provides an age model for the Mochras borehole. In addition, input of terrestrial organic matter in the sampled section is relatively high (van de Schootbrugge et al., 2005; Riding et al., 2013) and thus provides ideal material to study palaeo-fire regimes with a relatively high temporal constraint.

The Mochras core was drilled between 1967 and 1969 on the coast in northwest Wales, UK. Preserved 1 m length slabs of the core are stored at the British Geological Survey National Core Repository at Keyworth, UK. The Pliensbachian of Mochras shows alternating beds of pale grey limestone and dark brown to grey mudstone (Ruhl et al., 2016). These couplets occur throughout the Pliensbachian but vary in thickness, from about 90 cm at the Sinemurian–Pliensbachian boundary to about 30 cm in the Late Pliensbachian age strata, latest Margaritatus and Spinatum zones (Ruhl et al., 2016). The lithological couplets are well expressed around the SPB and in the Margaritatus Zone (Ruhl et al., 2016). For this study, samples were taken at an average sample spacing of 90 cm across the Sinemurian–Pliensbachian boundary (1272–1233 m b.s., metres below surface). In addition, data published in Hollaar et al. (2021, 2023) from the Late Pliensbachian interval that are sampled at a 10 cm (951–934 m b.s.) resolution and a 30 cm (934–918 m b.s.) resolution were utilized in this study. The macrocharcoal data between 934 and 918 m b.s. are new and have not previously been published. An overview of the number of samples per stratigraphic interval and proxy type can be found in Table S1 in the Supplement.

#### 2.1.2 Palaeo-location and provenance

During the Early Jurassic, the Mochras site was situated in the Boreal realm of the Laurasian Seaway, which contained an island archipelago and covers most of present-day northwestern and western Europe. The Mochras site lay at a palaeo-latitude of $\sim 35^{\circ}$ N (Torsvik and Cocks, 2017), just off the Welsh Massif in a relatively deep marine setting below storm wave base (Pieńkowski et al., 2021) but with a strong terrestrial influence (van de Schootbrugge et al., 2005; Riding et al., 2013; Xu et al., 2018; Storm et al., 2020).

The Welsh Massif was likely the main detrital source for the Cardigan Bay basin (Deconinck et al., 2019), although

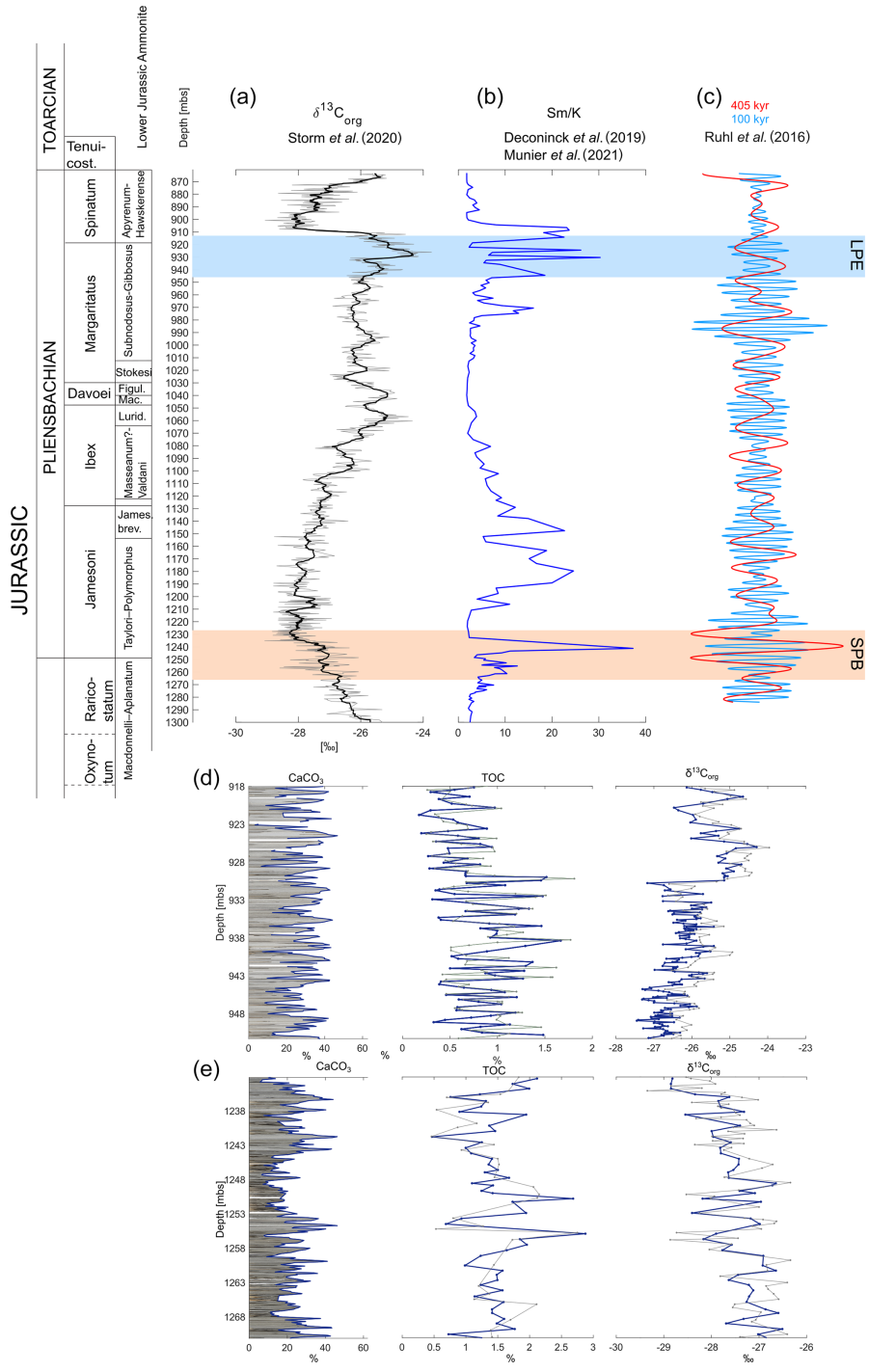


**Figure 1.** Cyclostratigraphic framework of the latest Sinemurian–Pliensbachian of the Mochras core and the two intervals studied here. The red bar represents the interval (1271–1233 m below surface, m b.s.) of the SPB, and the blue bar represents the interval of the LPE (951–918 m b.s.). **(a)** The $\delta^{13}C_{org}$ record from the Mochras core (Storm et al., 2020) shows the broad, negative carbon-isotope trend around the SPB and the positive carbon-isotope excursion (CIE) in the Late Pliensbachian. **(b)** The smectite / kaolinite (Sm/K) ratio reflects changes in the hydrological cycle, data from Deconinck et al. (2019) and Munier et al. (2021). Peaks in smectite indicate greater climatic aridity (Deconinck et al., 2019; Munier et al., 2021). **(c)** The bandpass-filtered Ca-elemental record in the depth domain from Ruhl et al. (2016) representing the 100 and 405 kyr cycles. **(d)** The LPE interval is carbonate-rich and shows the metre-scale variations in $CaCO_3$ and TOC next to the $\delta^{13}C_{org}$ positive shifts that mark the onset of the LPE. **(e)** The SPB interval contains relatively more clay, and lithological couplets of alternating $CaCO_3$- and TOC-enhanced beds occur on a metre scale. The $\delta^{13}C_{org}$ shows the negative trend of the long-negative limb of the SPB negative CIE.

other emergent areas in proximity likely also contributed (Deconinck et al., 2019). The nearby Irish Massif, situated west of the Welsh Massif, also cannot be dismissed as a source of nutrients, terrestrial organic particles, clay, and coarser mineral grains to the Cardigan Bay basin (Deconinck et al., 2019). Another possible source area is the emergent land of the Scottish Massif to the north of the Mochras Borehole and the London–Brabant Massif to the east of the Mochras Borehole (van de Schootbrugge et al., 2005).

Multiple nearby landmasses contributing runoff to the relatively deeper marine depositional environment allowed the charcoal record presented here to reflect a regional expression of multiple likely fires. These fires might have in part occurred synchronously, but it is also important to note that one stratigraphic rock sample in this study represents a $\sim 2$ kyr average signal, which is likely more than the fire return interval at the time of deposition and thus represents an averaging of the overall fire signal through time and space. Therefore, the term "fire activity" here describes the overall occurrences as increases and decreases in wildfires across the region.

In this study, we measure the abundance of micro-charcoal and macro-charcoal as a proxies for fire activity. The size of charcoal fragments is often used as an indicator of whether the fires were proximal or distal to the deposition site. Often larger, more proximal charcoal particles are found in terrestrial biomes and their depositional environments: in soils, lakes, and mires. In contrast, smaller charcoal particles that are windblown could potentially end up in a marine environment as well as in more distal terrestrial settings. However, experimental research has shown that riverine transport has the potential to carry the larger charcoal particles further away from shore, with the smaller charcoal particles becoming water saturated at a shorter distance and settling down closer to the shoreline (Nichols et al., 2000). In addition to this, other studies have indicated that larger charcoal particles (up to 7 cm) can be windblown and can travel up to 50 km from the original source, depending mainly on their morphology (Woodward and Haines, 2020). Combined, charcoal size, shape, and properties; wind direction; plume height; and riverine and marine transportation all have different impacts on the travel distances of different charcoal size classes. Hence, in the context of this study, no inferences can be made about the different size classes, and therefore micro-charcoal and macro-charcoal both serve as overall indicators of fire activity.

## 2.2 Methods

### 2.2.1 Mass spectrometry of $\delta^{13}C_{org}$, TOC, and $CaCO_3$

Bulk organic carbon isotopes, TOC, and carbonate content were measured to track changes in the carbon cycle and changes in total organic matter during the interval studied. 50 samples for the SPB interval (1271–1233 m b.s.) and 193 samples for the LPE (918–951 m b.s.) were processed for carbon isotope mass spectrometry. Bulk rock samples were powdered using a mortar and pestle, weighed into centrifuge tubes, and decarbonated using 3.3 % HCl. Following this, the samples were transferred to a hot bath (79 °C) for 1 h to remove siderite and dolomite. After this, the samples were centrifuged and the liquid decanted; this step was repeated (on average 2 times) until the samples were neutralized. Finally, the samples were oven dried, re-powdered, and weighed (to measure $CaCO_3$ loss) and transferred into small tin capsules for mass spectrometry (TOC and $\delta^{13}C_{org}$) at the University of Exeter, Penryn Campus.

### 2.2.2 Charcoal quantification and palynofacies

For the SPB interval, 54 samples were prepared for charcoal analysis and 42 for palynofacies at the University of Exeter, Streatham Campus. For the LPE interval, an additional 50 macro-charcoal samples were analysed to complement a total of 204 macro-charcoal samples for this interval. A total of 162 samples for palynofacies and 200 micro-charcoal samples were included in the LPE study interval.

Rock samples of 10–30 g weights were split into 0.5 $cm^3$ fragments to minimize the breakage of the organic particles while optimizing the surface area for palynological acid maceration. First, the 190 samples were treated with 10 % and 37 % HCl to remove carbonate. After this, hydrofluoric acid (40 % HF) was added to remove silicates from the samples. The samples were left to digest for 48 h, after which cold, concentrated HCl (37 %) was added to avoid calcium fluoride precipitation. Each sample was left to settle, after which it was decanted and topped up with deionized (DI) water, a step that was repeated $\sim$ six times in order to allow the sample to neutralize.

After neutralizing, five droplets of the mixed residue were taken for the analysis of palynofacies (total particulate organic matter) prior to any sieving. The remaining residue was sieved through a 125 µm sieve and a 10 µm sieve to retrieve the macroscopic fraction (> 125 µm) and microscopic fraction (10–125 µm). Macroscopic charcoal (> 125 µm) was quantified using a Zeiss Stemi microscope with a $10 \times 4$ magnification lens and top lighting from a "goose-necked" light source. The entire macroscopic fraction was dispersed in a Petri dish filled with DI water, and the number of charcoal particles were counted and expressed per 10 g of processed rock. In some samples, large clusters of matrix were not digested by the acid, in which case they were taken out and dry weighed to deduce the weight of the total processed rock. Charcoal particles are identified as being opaque, black, angular, reflective of light, and elongated; having a lustrous shine; lacking brown edges; prone to splintering during breakage; and often showing the anatomical structure of the plant preserved (Fig. S1 and Table S2, Scott, 2000; Scott and Damblon, 2010).

Microscopic charcoal (10–125 µm) was analysed on a palynological slide. A known quantity of 125 µL of the mi-

croscopic fraction was mounted onto microscopic slides using glycerine jelly. A transmitted light microscope (Olympus; BX53) with $40 \times 10$ magnification was used to count the charcoal particles. Four transects per slide were counted: one transect on the left, two in the middle, and one on the right of the coverslip. These data were then scaled up to the known quantity of the total sample (Belcher et al., 2005). Palynofacies were examined to record shifts in the type of organic matter (terrestrial vs. marine) and potential changes in organic matter preservation and/or terrestrial runoff. Palynofacies were quantified using the optical light microscope, and a minimum of 300 organic particles per palynological slide were counted. The types of organic matter were roughly grouped following Oboh-Ikuenobe et al. (2005): terrestrial palynomorphs (spores and pollen), marine palynomorphs (dinoflagellates, acritarchs, prasinophytes, and foraminifera test linings), fungal remains, structured phytoclasts (wood particles and parenchyma), unstructured phytoclasts (degraded plant remains), charcoal, black debris (palynomorphs filled with pyrite), and amorphous organic matter (AOM; fluffy, clotted, and granular masses, with colour ranging from almost colourless to yellow and pale brown).

#### 2.2.3 X-ray diffraction (XRD) clay mineralogy

A total of 55 samples were prepared for clay mineralogy spanning the SPB interval, and 194 samples were prepared for the LPE interval. About 5 g of bulk-rock sample was gently crushed and powdered with an agate mortar, after which about 2–3 g of the powdered sample was decarbonated with a 0.2 M HCl solution. The samples were left to settle for 95 min, after which the suspended clay-sized fraction ($< 2\,\mu m$) was extracted with a syringe (following Stokes' law). The clay fraction was centrifuged and subsequently smeared and oriented on glass slides. The samples were analysed by X-ray diffraction (XRD) using a Bruker D4 Endeavour diffractometer (Bruker, Billerica, MA, USA) with Cu K$\alpha$ radiation, LynxEye detector, and Ni filter under 40 kV voltage and 25 mA intensity at the Biogéosciences laboratory, Université Bourgogne/FrancheComté, Dijon. Three runs were performed per sample to discriminate between the clay phases: (1) air drying at room temperature, (2) ethyleneglycol solvation for 24 h, and (3) heating at 490 °C for 2 h, following Moore and Reynolds (1997). Comparing the three diffractograms obtained, the clay minerals were identified using their main diffraction (d001) peaks. The proportions of each clay mineral on glycolated diffractograms were estimated using the MACDIFF 4.2.5 software (Petschick, 2000). The identification of the clay minerals further follows the methods in Moore and Reynolds (1997) and Deconinck et al. (2019).

#### 2.2.4 Statistical analysis

**Orbital filters and the charcoal record**

The Pliensbachian of the Mochras core has a well-established astrochronological framework (Ruhl et al., 2016; Hinnov et al., 2018; Storm et al., 2020; Hollaar et al., 2021; Pienkowski et al., 2021). Based on the existing cyclostratigraphy, the 100 kyr eccentricity cycle lies within the range of 3.2–10.2 m (Ruhl et al., 2016; Hinnov et al., 2018), 6.3–4.8 m (Storm et al., 2020), or $\sim$5.3 m (Pieńkowski et al., 2021) for the SPB and LPE intervals studied here. These intervals each comprise $\sim$7–8 short eccentricity cycles. No spectral analysis has been performed on the records presented here because of the limited time span represented. Instead, we visually compare the charcoal and clay records to the 100 and 405 kyr filters based on Ca and Ti (Ruhl et al., 2016; Hinnov et al., 2018). In Fig. S2 in the Supplement, we lay the 3.2–10 m filter (based on Ruhl et al., 2016) derived from the macro-charcoal record over the normalized dataset of the macro-charcoal record.

**Pearson correlation**

A Pearson correlation was used to test for possible correlation between the charcoal abundance (both size fractions) and palynofacies, as well as the significance, using RMatlab2021b (The MathWorks Inc., 2021). The $p$ value tests the hypothesis of no correlation against the alternative hypothesis of a positive or negative correlation, with a significance level of $\alpha = 0.05$. See Fig. S3 in the Supplement.

**Wilcoxon test**

A Wilcoxon rank-sum test was performed in RMatlab2023b (The MathWorks Inc., 2023) to test the null hypothesis of equal means between the charcoal populations of the LPE and the SPB intervals with a significance level of $\alpha = 0.05$. The test was performed separately for the macro-charcoal and micro-charcoal records.

**Principal component analysis (PCA)**

Principal component analysis (PCA) was performed to explore the potential covariance of charcoal, clay mineralogy, palynofacies, and mass-spectrometry records for the two studied intervals. This was executed in the software PAST (Hammer et al., 2001) on the normalized dataset (macro-charcoal, micro-charcoal, TOC, $CaCO_3$, $\delta^{13}C_{org}$, S/I, Sm/K, K/I, and phytoclasts).

## 3 Results

The data presented here that cover the run-up to and onset of the SPB (1271–1233 m b.s.) show a $\sim$1.8 ‰ negative shift in $\delta^{13}C_{org}$ spanning the end of the negative CIE limb in the

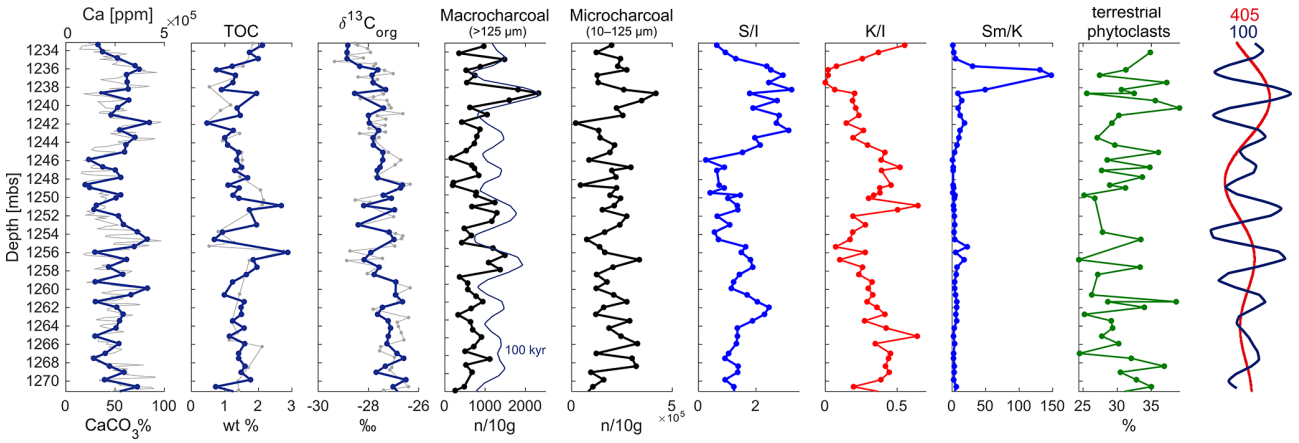


**Figure 2.** The SPB interval studied showing all proxies in this study in the context of the orbital filters (Ruhl et al., 2016). The $CaCO_3$, TOC, and $\delta^{13}C_{org}$ (blue) data obtained in the present study are plotted over previously published data (light grey – Ruhl et al., 2016; Storm et al., 2020). The macro-charcoal abundance shows ∼ eight increases and decreases throughout the studied interval. These high–low intervals in the macro-charcoal record correspond to the 100 kyr filter (blue; see also Fig. S2). The majority of macro-charcoal peaks are mirrored in the micro-charcoal fraction. Alternating phases of increase in the smectite / illite ratio (S/I) and the kaolinite / illite ratio (K/I) indicate swings in the hydrological cycle. This is further indicated by the smectite / kaolinite ratio (Sm/K). The percentage of terrestrial phytoclasts shows that the terrestrially sourced organic particles fluctuate around 30 % in the studied interval. Finally, the bandpass-filtered time series of the Ca-elemental XRF record of Ruhl et al. (2016) indicate that the clay records shift dominance on a 405 kyr timescale. The peaks in the macro-charcoal record occur on a 100 kyr timescale (see also Fig. S2).

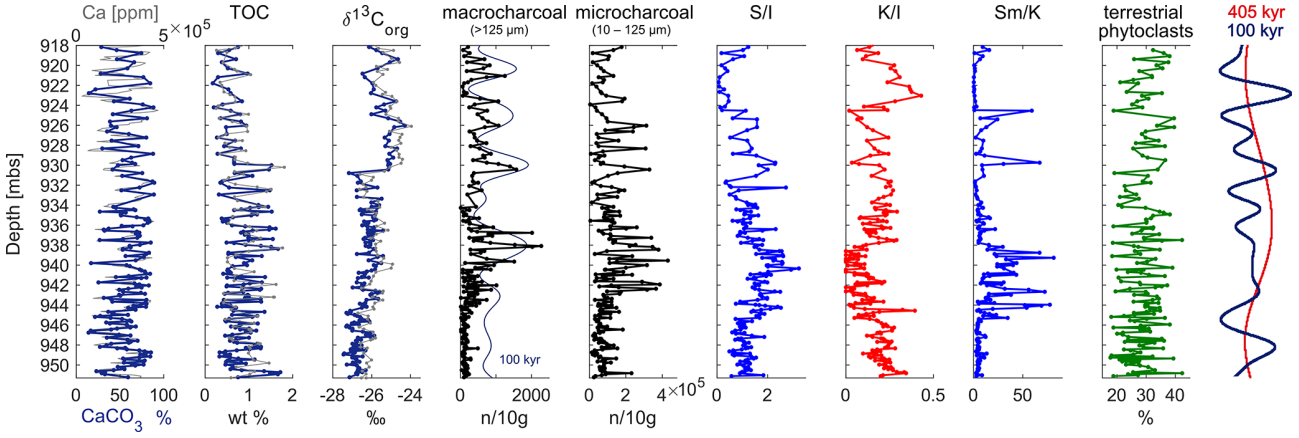


**Figure 3.** Synthesis of the LPE interval showing all proxies considered in this study in the context of the orbital filters (Ruhl et al., 2016). The $CaCO_3$, TOC, and $\delta^{13}C_{org}$ (blue) from Hollaar et al. (2023) are plotted over independently generated data (light grey – Ruhl et al., 2016; Storm et al., 2020). The macro-charcoal abundance shows ∼ seven peaks throughout the studied interval. These seven increases and decreases in macro-charcoal abundance correspond to the 100 kyr eccentricity (blue; see also Fig. S2). The majority of macro-charcoal peaks are mirrored in the micro-charcoal fraction. Alternating phases of increase in the smectite / illite ratio (S/I) and the kaolinite / illite ratio (K/I) indicate swings in the hydrological cycle. This is further indicated by the smectite / kaolinite ratio (Sm/K). The percentage of terrestrial phytoclasts shows that the terrestrially sourced organic particles fluctuate around 30 % in the studied interval. Finally, the orbital filters of Ruhl et al. (2016) are placed next to the proxy records. This shows that the clay records shift dominance on a 405 kyr timescale. The peaks in the macro-charcoal record occur on a 100 kyr timescale.

Mochras borehole and reaching most negative values. The results of the LPE interval, which encompass the run-up and onset of the LPE (951–918 m b.s.), show a rapid positive shift in the $\delta^{13}C_{org}$ of ∼ 1.8 ‰ (between 930.8 and 930.4 m b.s., in agreement with Storm et al., 2020).

Large fluctuations are observed in the abundance of macroscopic (> 125 µm) and microscopic (10–125 µm) fossil charcoal for both CIEs. For the SPB, micro-charcoal abundance fluctuates from $2 \times 10^4$ to $4.2 \times 10^5$ (mean $2 \times 10^5$) particles per 10 g of sediment, and the number of macro-charcoal particles varies from 99 to 2327 (mean 787) par-

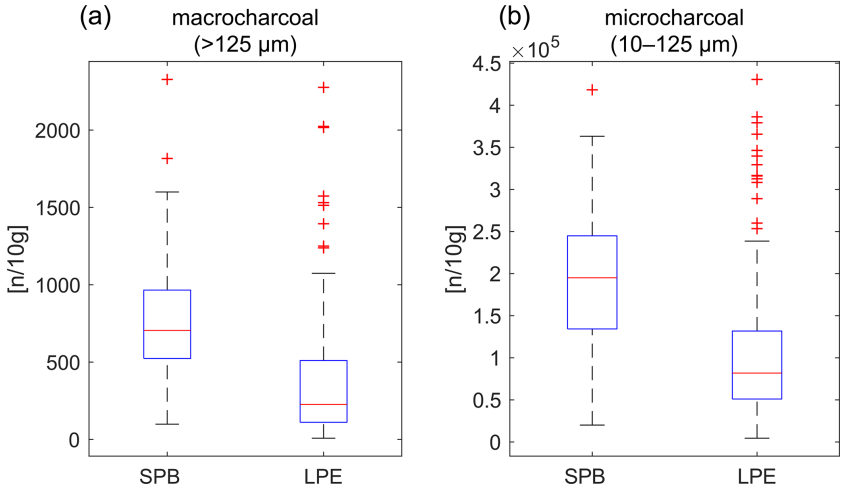


**Figure 4.** Distribution box plots of the macro-charcoal and micro-charcoal abundance of the SPB and LPE intervals studied. **(a)** Average macro-charcoal abundance is higher in the SPB interval compared to the LPE interval; however, the absolute minimum and maximum are similar. **(b)** Average micro-charcoal abundance is higher for the SPB compared to the LPE. The minimum number of micro-charcoal particles is lower for the LPE; however, the absolute minimum and maximum are similar for both intervals.

ticles per 10 g sediment (Fig. 2, Table S3 in the Supplement). A similar trend is observed in both size fractions, with individual charcoal peaks fluctuating on a 2–4 m scale (Fig. 2). In the higher-resolution LPE interval, metre-scale individual peaks of charcoal abundance are observed, with micro-charcoal abundance fluctuating from $4.5 \times 10^3$ to $4.3 \times 10^5$ (mean $1.1 \times 10^5$) particles per 10 g of sediment, and the number of macro-charcoal particles varies from 8 to 2276 (mean 376) particles per 10 g sediment (Fig. 3, Table S3). Longer-term fluctuations in the macro-charcoal record are also observed, with bundling of peaks visible every $\sim$ 4–5 m. Micro- and macro-charcoal are more abundant in the SPB compared to the LPE (Fig. 4). The outcome of the Wilcoxon signed-rank test confirms different medians of the SPB and LPE macro-charcoal (null hypothesis, $H_0$ rejected; $p < 0.001$) and micro-charcoal ($H_0$ rejected; $p < 0.001$).

The palynofacies of both intervals are typically marine (AOM > 58 %). The proportion of terrestrial vs. marine organic matter remains relatively stable through both the SPB and LPE, varying between 24.4 % and 39.1 % (mean 30.7 %), and 17.7 % and 42.3 % (mean 28.9 %), respectively. Charcoal accounts for $\sim$ 3.7 % and $\sim$ 4.5 % of the total particulate organic matter for the SPB and the LPE intervals, respectively (Fig. S4 in the Supplement). The abundance of macro-charcoal is not influenced by the percentage of terrestrial particulate organic matter through the SPB and LPE intervals (SPB $r = -0.12$, $p = 0.42$; LPE $r = 0.06$, $p = 0.46$) and neither is the micro-charcoal abundance for the SPB interval ($r = 0.07$, $p = 0.62$). However, a very weak correlation exists between the percentage of terrestrial phytoclasts and micro-charcoal abundance in the LPE interval ($r = 0.16$, $p = 0.05$). These results suggest that the preservation and/or influx of terrestrial particulate organic matter is not the main driver of fluctuations in charcoal abundance.

The clay mineral assemblages of the SPB and LPE are dominated by illite, kaolinite, and smectite (I-S R0), with smectite increasing in parallel to decreases in illite and kaolinite (Fig. S5 in the Supplement). Low proportions of chlorite and sparse I-S R1 are present in the SPB record. Chlorite and I-S R1 are generally low in the LPE record but increase between 924 and 219 m b.s. (Fig. S5). Two smectite-enhanced phases occur for the SPB at 1264–1255 and 1245–1235 m b.s. Both these phases are coeval with high charcoal abundance (both size fractions; Figs. 2 and S6 in the Supplement). Additionally, the LPE interval encompasses two stratigraphic intervals rich in smectite, from 944 to 937 and from 931 to 924 m b.s. Charcoal abundance (both size fractions) increases overall, increases coevally with the S/I over $\sim$ 5 m scale fluctuations, and decreases at levels with high K/I (Figs. 3 and S7 in the Supplement). The 3.2–10.2 m orbital filter of the macro-charcoal records (interpreted as the 100 kyr eccentricity; Ruhl et al., 2016; Hinnov et al., 2018; Storm et al., 2020; Pienkowski et al., 2021), indicates that the observed fluctuations in the macro-charcoal record occur with a 100 kyr periodicity (Fig. S2).

## 4 Discussion

### 4.1 Charcoal transport and preservation

The charcoal records for both the SPB interval and the LPE interval do not appear to be linked to the terrestrial influx of materials, as evidenced by the palynofacies. No correlation or covariance exists between the abundance of terrestrial phytoclasts and the number of charcoal particles,

which suggests that the abundance of charcoal is not a reflection of preservation and/or runoff changes. Inferred sea-level changes during the LPE and the SPB could potentially have impacted the charcoal abundance record and the clay mineralogy. Transgression and relative sea-level rise during the SPB has been extensively recorded in the Boreal and Tethys regions and in South America (e.g. Legarreta and Uliana, 1996; de Graciansky et al., 1998; Hesselbo and Jenkyns, 1998; Danisch et al., 2019; Silva et al., 2021). The Late Pliensbachian is characterized by widespread regressive facies and inferred relative sea-level fall, likely also indicating a closer proximity to shore of the Mochras borehole palaeo-environment. Fossil wood in the Mochras borehole has been shown to become more abundant at this time, suggesting a potential bias of higher terrestrial input from a nearby landmass (Ullmann et al., 2022). However, the mean abundance of macro-charcoal and micro-charcoal is higher in the Mochras borehole during the SPB (mean of 787 and $2 \times 10^5$, respectively) compared to the LPE (mean of 376 and $1.1 \times 10^5$, respectively), suggesting that the shore proximity did not impact overall charcoal abundance. Similarly, the palynofacies analysis indicates that the mean abundance of terrestrial particulate organic matter during the SPB (30.7 %) was not higher compared to the LPE (28.9 %). Hence, we take this as strong evidence that the record of fossil charcoal records changes in wildfire activity.

### 4.2 Orbital forcing of the hydrological cycle and fire

Alternations in the dominance of smectite and kaolinite occur approximately every 10 m in both the LPE record and the SPB record. Kaolinite and smectite reflect hydrological changes in the palaeo-environment of the Cardigan Bay basin (Deconinck et al., 2019; Munier et al., 2021). As the smectite and kaolinite clay minerals are detrital in character, and their abundance varies in opposition to one another (Figs. 2 and 3), these clays are likely derived from pedogenic weathering profiles (Deconinck et al., 2019). Smectite preferentially forms under a warm and seasonally arid climate, similar to a monsoonal climate system or the winter-wet climate of the Mediterranean zone (Chamley, 1989; Deconinck et al., 2019). Kaolinite is indicative of an accelerated hydrological cycle and an intensification of hydrolysis, increased runoff, and a year-round wet climate (Chamley, 1989; Ruffell et al., 2002) either via formation in strong weathering profiles or via the physical erosion of kaolinite-bearing rocks (Chamley, 1989). Pedogenic kaolinite preferentially forms in a hot climate (Chamley, 1989; Ruffell et al., 2002). At times of high smectite abundance, fire activity is greatest, as observed from the macroscopic and microscopic charcoal fractions (Figs. 2 and 3). Based on the astrochronological framework of the Mochras borehole (Ruhl et al., 2016; Hinnov et al., 2018; Storm et al., 2020; Pieńkowski et al., 2021), these alternations appear to occur in concert with the 405 kyr long eccentricity cycles (Figs. 2 and 3). Eccentricity modulates the precession-driven changes in seasonal and latitudinal distribution of insolation (Imbrie and Imbrie, 1980; Berger et al., 1989). One $\sim$ 20 kyr precession cycle can represent a strongly seasonal extreme climate for $\sim$ 10 kyr and a weakly seasonal climate for the subsequent $\sim$ 10 kyr. The geological record averages the amplification or suppression of seasonality between years (Fig. S8 in the Supplement). Eccentricity forcing modulates the amplitudes of these extremes in seasonality with periodicities of 100 and 405 kyr.

In the Mesozoic, eccentricity maxima are commonly associated with dry climates that are disrupted by short and intense periods of precipitation and storm activity in the boreal landmasses bordering the northwest Tethys (Martinez and Dera, 2015). In contrast, eccentricity minima are characterized by more moderate seasonal contrasts and year-round wet conditions (Martinez and Dera, 2015). Eccentricity minima are linked to periods of enhanced runoff and weathering conditions as evidenced by high kaolinite content, $^{87}Sr/^{86}Sr$, and negative shifts in $\delta^{18}O$ (Martinez and Dera, 2015). Therefore, we link the observed smectite-rich intervals to eccentricity maxima and the kaolinite-rich intervals to eccentricity minima. Charcoal abundance is highest during the seasonal climate of the eccentricity maxima for the SPB (Figs. 2 and 3), in agreement with the previous findings for the LPE (Hollaar et al., 2021, 2023).

Both the LPE and the SPB study intervals span two 405 kyr cycles (Ruhl et al., 2016; Hinnov et al., 2018; Storm et al., 2020; Pieńkowksi et al., 2021). The relative abundance of smectite and the abundance of charcoal both reach a peak during the maxima in the long eccentricity cycle, supporting the notion that orbitally driven changes in seasonal contrast in hydrolysis led to high fire activity. Within these long-term trends, the macro-charcoal record also shows $\sim$ 5 m scale individual peaks or clusters in both the LPE record and the SPB record (Figs. S2, 2 and 3). Based on the existing age model (Ruhl et al., 2016; Hinnov et al., 2018; Storm et al., 2020; Pieńkowksi et al., 2021), we deduce that this is the expression of the $\sim$ 100 kyr eccentricity cycle in the macro-charcoal record. The bandpass-filtered time series representing the $\sim$ 100 kyr cycle in the Pliensbachian of the Mochras core (derived from the Ca and macro-charcoal records) captures the observed $\sim$ 5 m oscillations in the fire record (Figs. S2, 2, and 3 and Ruhl et al., 2016; Hinnov et al., 2018; Storm et al., 2020; Pieńkowski et al., 2021).

The Sinemurian–Pliensbachian transition is generally associated with an overall warm and humid climate (Korte and Hesselbo, 2011; Gómez et al., 2016) and with enhanced levels of runoff and weathering (Bougeault et al., 2017). The results presented here suggest that within this overall warm and humid background, orbital forcing created year-round wet periods that were not conducive to frequent fire, alternating with periods that remained warm but had a more seasonal climate that allowed for ignition during the dry season. In contrast, the LPE and the sediments of the late Margaritatus ammonite chronozone formed in an overall semi-arid

climate with proposed lower runoff levels from the land into the sea (Deconinck et al., 2019; Hollaar et al., 2021, 2023). During the run-up of the LPE, we infer orbitally forced alternating climatic states of more extreme seasonality (high fire and smectite) and a more equitable year-round wet climate (low fire and high kaolinite; Hollaar et al., 2021, 2023) acting within this overall semi-arid climate phase. Overall, kaolinite fluctuates in abundance in opposition to smectite, reflecting hydrological changes from wet and hot to semi-arid and hot, in agreement with high fire activity during a seasonal climate and fire suppression during a year-round wet climate in both the LPE and the SPB.

### 4.3 Vegetation, fire, and the intermediate fire–productivity gradient

Fuel (vegetation biomass) and moisture status of the fuel, as governed by seasonal patterns in precipitation and temperature, are the core factors that influence fire behaviour and fire regime (Archibald et al., 2009, 2013, 2018; Cochrane and Ryan, 2009; Bradstock, 2010; Bowman et al., 2014). Ecosystems with limited wildfire activity are generally associated either with high precipitation and abundant primary productivity or with low productivity under strongly arid conditions (Pausas and Paula, 2012). In contrast, high wildfire activity occurs in climates that are in the middle of the productivity gradient, where during moist periods plant growth is rapid and biomass builds up, forming a connected fuel structure. When followed by periods of drought, the fuel moisture content is lowered, enabling fire ignition and spread (Pausas and Paula, 2012). Additionally, higher sensitivity to fuel moisture levels in the tropical or mesic areas has been noted, where a small fall in fuel moisture content can lead to more flammable conditions (Cochrane, 2003), such that the midpoints in the intermediate fire–productivity gradient are further enhanced. The intermediate fire–productivity hypothesis (Pausas and Bradstock, 2007; Pausas and Ribeiro, 2013) conceptualizes this relationship between climate–vegetation–fire, where fire activity is plotted along an aridity and productivity gradient (Fig. 5).

The observed alternating modes of high and low fire activity, as inferred from the Lower Jurassic fossil charcoal record during the onset of the SPB and LPE, likely indicate shifts in seasonality of the Cardigan Bay basin hinterland and would place both the LPE and the SPB at intermediate-productivity levels during maximum eccentricity forcing. The combined deep-time fire and hydrological records we present here are in agreement with the intermediate-productivity hypothesis of Pausas and Bradstock (2007) and indicate that even very different plant functional types and different vegetation assemblages, e.g. a world without grasses, were still subject to this overall fire–productivity-gradient control. We indicate in Fig. 5 how these ecosystems without grasses or other flowering plants may have looked with respect to typical Jurassic fuel compositions. We suggest that both the LPE and the SPB switched between a state of low fire (limited either by climatic aridity or by the presence and connectivity of fuel) and a state of high fire during which seasonal contrast is high and an ideal "fire window" exists in which biomass builds up during the wet season and a fire-prone season follows (Fig. 5).

The Early Jurassic time interval studied likely had five distinct biomes: a seasonal dry (summer-wet or subtropical) biome in the low latitudes, a desert biome in the subtropics, narrow latitudinal bands of a winter-wet biome at low–mid latitude, and warm-temperate and cool-temperate biomes at midlatitudes and high-latitudes, respectively (Rees et al., 2000; Willis and McElwain, 2013). The Cardigan Bay basin was likely positioned within the winter-wet biome at approximately 35° N (Torsvik and Cox, 2017). It therefore would have sat within the bounds of the fire window of the intermediate fire–productivity hypothesis (Fig. 5). The winter-wet biome in both the Sinemurian stage and the Pliensbachian stage was dominated by conifers as the canopy tree, with a mid-canopy vegetation of cycads and tree-ferns and an understorey mixture of seed ferns, horsetails, and ferns that likely flourished during wetter periods (Rees et al., 2000; Slater et al., 2019; Bos et al., 2023). This is evidenced from sporomorph data from the Mochras borehole that hosts abundant fossil pollen from the Sinemurian and Pliensbachian ($> 94\,\%$; Van de Schootbrugge et al., 2005). Additionally, nearby locations also show evidence of orbitally paced shifts in vegetation assemblages from sites at St. Audries Bay, UK, and in northwestern Germany (Bonis et al., 2010; Bos et al., 2023).

During the 100 kyr eccentricity maxima in the UK, pollen from the dry-adapted cheirolepidacean conifers was found to be highly abundant (Bonis et al., 2010), while in Germany a mire-conifer community is apparent, with sporomorphs indicating variations in abundance of ferns and fern allies occurring over a 405 kyr eccentricity cycle and with ferns most abundant during eccentricity maxima (Bos et al., 2023).

Dry-adapted vegetation such as the cheirolepidacean conifers likely thrived during more extreme seasonal droughts, maintaining biomass. In contrast, ferns and fern allies (and mire-conifers as humid-loving plants) would grow rapidly during sustained year-round periods of rainfall (eccentricity minima), likely both inhabiting open environments and colonizing the understorey of conifer forests. Furthermore, these humid-loving plants would also have been able to build dense, connected fuel loads during the wet season of eccentricity maxima, which were then readily dried during the annual dry season. Ferns, when cured, carry high-intensity fires (Adie et al., 2011; Belcher and Hudspith, 2017), and during the Mesozoic "fern prairies" have been linked to intense surface fires (Harris, 1981; Van Konijnenburg-Van Cittert, 2002; Collinson et al., 2007, 2009). Hence, they are suggested to have functioned in a similar fashion to grasslands and fern stands today in terms of supporting fires; Mesozoic fern prairies and savannahs therefore likely filled a similar ecological niche to grasses in the modern day (Belcher et al.,

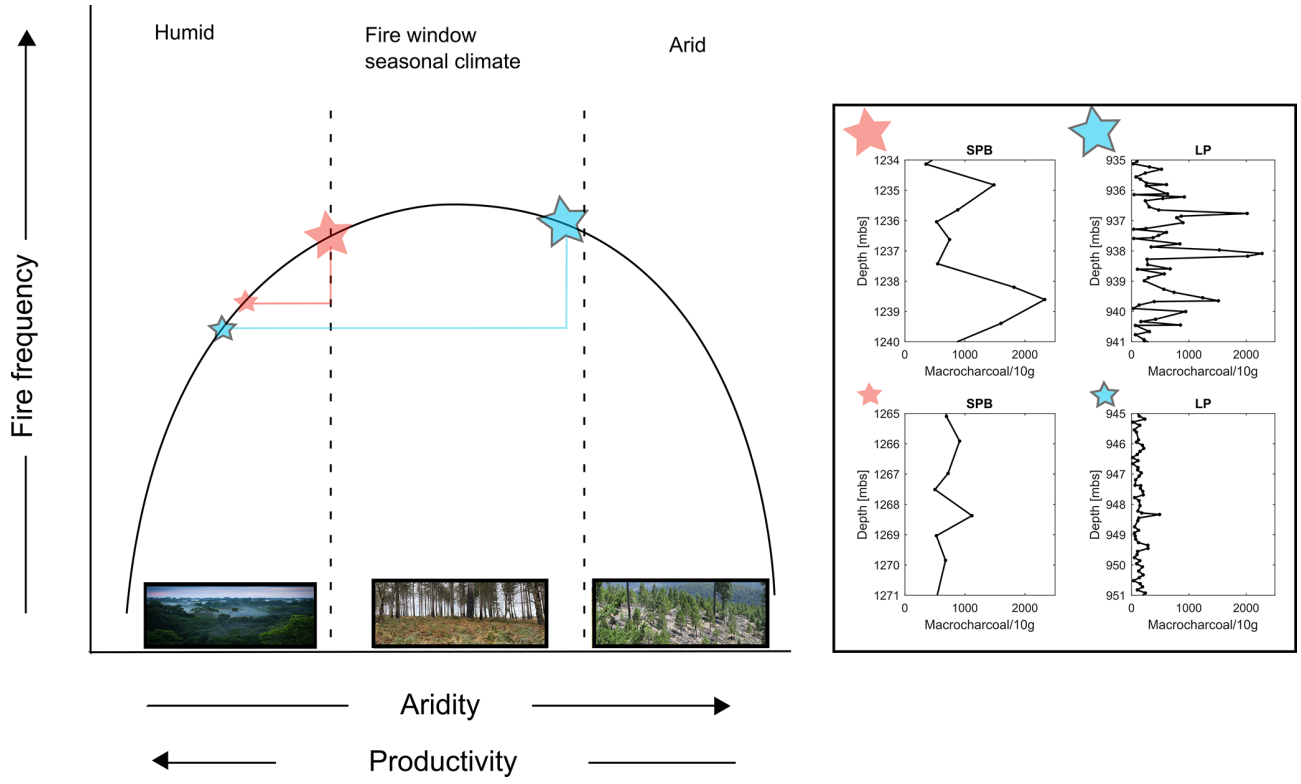


**Figure 5.** The LPE and SPB fire records placed on the intermediate-productivity gradient. The graph is adapted from Pausas and Bradstock (2007). Fire frequency is highest in the middle of the hyperbola; medium levels of aridity and productivity created a seasonal climate in which seasonal biomass growth was possible (productivity), and seasonally the fuel moisture limits were lower in a season of drought (aridity), creating the optimized "fire window". The SPB is plotted on this fire–productivity gradient in red: the small star indicates the eccentricity minimum state, and the large star the eccentricity maximum state. The LPE is plotted on the fire–productivity gradient in blue, and again the small star indicates the eccentricity minimum, and the large star the eccentricity maximum. The LPE has a larger range compared to the SPB, experienced more fire suppression due to high humidity levels during eccentricity minima, and was also closer to a productivity limitation state during the eccentricity maximum.

2013, and references therein). Ferns are indeed a common feature of Mesozoic charcoal assemblages, showing their association with fire throughout time (e.g. Collinson et al., 2000; Brown et al., 2012).

In the present day, temperature is an important regulator of fire occurrence. While dead fuel moisture (e.g. that of litter and cured herbaceous components) is primarily influenced by the variability in relative humidity, live fuels are controlled by the combination of temperature and moisture availability, where long periods of drought or heat wave extremes can strongly influence their flammability. Sea-surface temperatures during the Sinemurian and Pliensbachian were apparently higher than 28 °C at times (Robinson et al., 2017). But high-resolution temperature reconstructions are lacking for the Early Jurassic. Orbital forcing of regional–global seawater temperatures occurred throughout the Cenozoic (Westerhold et al., 2020) and likely also the Mesozoic; however, the climate response to changes in orbital insolation is nonlinear, and the mean annual insolation is not impacted by precession (Rubicam, 1994). Therefore, the biomes of the SPB existed in an overall warm world that was characterized by background orbitally driven climate shifts across the moister side of the fire–productivity gradient, but superimposed on this, live fuels were also responsive to extreme weather linked to periods of drought and heat.

We propose that the overall humid climate of the SPB fits the high-productivity scenario, in which the frequency of flammable conditions is the main factor controlling fire occurrence. No evidence was found to place the SPB on the productivity-limiting high-aridity side of the fire–productivity gradient, where fire frequency would have been mainly influenced by enhanced rainfall in an otherwise dry climate. These findings are in line with the presence of plant cuticle through the studied record, indicating the presence of vegetation throughout this time period and during high and low modes of fire activity. Hence, the SPB seems to conform to the humid and high-productivity end of the aridity gradient (Fig. 5; red lines). Within these constraints (Fig. 5), the SPB is characterized by two likely states across the fire–productivity gradient. The biome was situated at the wet-

ter, low-fire side of the fire–productivity gradient during eccentricity minima (Fig. 5) and at the seasonal, high-fire end of the fire–productivity gradient during eccentricity maxima (but only for each precession half-cycle; Fig. 5).

The fluctuations detected in the present study for the SPB occurred over both long eccentricity and short eccentricity timescales in the macro-charcoal record, showing longer phases of overall enhancement of fire (405 kyr eccentricity) and relatively abrupt shifts from low to high fire and back again ($\sim$ 100 kyr eccentricity). For this reason, the SPB is placed on a steep portion of the fire–productivity-gradient curve (Fig. 5). Overall, the mean charcoal abundance is relatively high, and no sustained periods of very low charcoal abundance are observed in the SPB record, which indicates that the climate never became too wet to fully limit fire activity at that time.

The Late Pliensbachian has been linked to a global cooling event, with a potential 5–7 °C lowering in temperature inferred for the northwest Tethys region (Korte et al., 2015). The atmospheric-moisture-holding capacity of a cooler climate is lower compared to a warm climate, in which 1 °C of cooling likely lowers the water-holding capacity of air by 7 % (Trenberth et al., 2005). The presence of terrestrial phytoclasts throughout confirms the presence of vegetation in the surrounding landmasses throughout this period. The mean abundance of charcoal for the LPE section is slightly lower than that of the SPB, and the lowest charcoal abundances are coeval with a K/I enhancement, suggesting that during eccentricity minima, environmental conditions moved further into the humid zone of the fire–productivity gradient (Fig. 5; blue line). Increasing eccentricity shifted the system to a more seasonal climate where the fire and clay records indicate the presence of a wet season that allowed for buildup of biomass followed by a dry season in which fire was able to ignite and spread.

Conceptually, the relatively drier and cooler LPE climate would have resulted in conditions that are more arid, shifting to the biomass-limited part of the fire–productivity gradient during eccentricity maxima compared to the SPB (Fig. 5; blue lines). This is supported by the large fluctuations observed between low fire frequency and high fire frequency for the LPE and by the fact that estimated high fire periods did not occur suddenly but rather were sustained over a larger part of the cycle. Therefore, the phase of highest fire frequency operating in the seasonal "fire window" as indicated in Fig. 5 for the LPE (blue lines) likely occurred for a larger part of the fire–productivity gradient. Hence, conditions across the LPE occurred across a wider range of the fire–productivity gradient (Fig. 5 blue lines) compared to the SPB. There is no evidence that conditions ever became limited by aridity, and conditions during the LPE did not extend beyond the seasonal fire window into the arid part of the fire–productivity gradient.

Importantly, the Jurassic climate was overall warm and humid, about 5–10 °C warmer on a global average compared to today (e.g. Rees et al., 2000; Sellwood and Valdes, 2008), with $\sim$ 3.5–10 times the pre-industrial value of atmospheric $pCO_2$ during the Early Jurassic (e.g. Retallack, 2001; Beerling and Royer, 2002; McElwain et al., 2005; Berner, 2006; Steinthorsdottir and Vajda, 2015; Li et al., 2020). In this context, it may not be surprising that a relative cooling event in the Early Jurassic did not lead to the aridity and biomass-limiting conditions observed during the last glacial period at latitudes of $\sim$ 38° N (Daniau et al., 2007).

## 5 Conclusions

The study of two different climatic "background" states during the LPE and the SPB shows that fire activity was strongly modulated by orbital eccentricity cycles. The 405 kyr shifts in the record of wildfire prevalence reflect similar changes in the hydrological cycle (based on clay mineralogy data), showing that high fire activity occurred during periods of high seasonal contrast and that fire activity was suppressed during periods of high year-round humidity because the latter would have enhanced the fuel moisture levels and prevented frequent ignition and sustained fire spread. The fire record of both climatic events is limited by the high fuel moisture levels during eccentricity minima, but fires were more prevalent during times of increased seasonality every precession half-cycle during eccentricity maxima. Hence, during both events, fire activity was limited by fuel moisture content and not by productivity. The SPB and the LPE climate systems were therefore both situated on the moisture-limited side of the intermediate fire–productivity gradient (Fig. 5). Due to the lower-moisture-holding capacity of cold air, the overall higher seasonality of the Late Pliensbachian, and the more sustained high fire frequency periods (based on the charcoal record for the LPE) we place the LPE towards the higher end of the aridity gradient, within the maximum seasonality and maximum fire frequency window of the fire productivity graph (Fig. 5). The SPB fire regime reflected a more humid climate that shifted abruptly between low fire frequency and high fire frequency within less extreme bounds on the aridity gradient. This research reveals that the intermediate fire–productivity hypothesis (Pausas and Bradstock, 2007) can also be applied to high-resolution deep time records before the evolution of grasses and that this hypothesis explains the influence of orbital cycles within different overall climate states well, be they cooling or warming trends. The coupling of high-resolution clay mineralogy and fossil charcoal records, combined with constraints on orbital forcing at such a time, allows for inferences as to how Earth's natural climate state variability has driven shifts in terrestrial productivity through the geological past.

*Data availability.* Supplementary data are available from the National Geoscience Data Centre at Keyworth (NGDC) at https://doi.org/10.5285/1461dbe5-50a8-425c-8c49-ac1f04bcc271 (Hollaar, 2022) for the interval 934–918 m b.s. All data presented for the interval 951–934 m b.s. are available from the National Geoscience Data Centre at Keyworth (NGDC) at https://doi.org/10.5285/d6b7c567-49f0-44c7-a94c-e82fa17ff98e (Hollaar, 2021). All data for the interval 1271–1233 m b.s. are available from the National Geoscience Data Centre at Keyworth (NGDC) at DOI https://doi.org/10.5285/2ec864e0-cb08-44c0-92fe-07af2ef93e3a (Hollaar, 2024).

*Supplement.* The supplement related to this article is available online at: https://doi.org/10.5194/bg-21-2795-2024-supplement.

*Author contributions.* All the authors contributed to the investigation. The project was conceptualized by CMB and SPH. Funding was acquired by SPH and CMB. All authors developed and co-ordinated the project methodology. TH created the original manuscript draft. All authors contributed to the interpretation, review, and editing of the final paper.

*Competing interests.* The contact author has declared that none of the authors has any competing interests.

*Disclaimer.* Publisher's note: Copernicus Publications remains neutral with regard to jurisdictional claims made in the text, published maps, institutional affiliations, or any other geographical representation in this paper. While Copernicus Publications makes every effort to include appropriate place names, the final responsibility lies with the authors.

*Acknowledgements.* This is a contribution to the Early Jurassic Earth System and Timescale (JET) project. We warmly thank all project participants for fruitful discussion over the course of this research. The staff at the National Core Repository at the British Geological Survey, Keyworth, are especially thanked for their help supporting work on the core.

*Financial support.* This research has been directly supported by the Natural Environment Research Council (grant no. NE/N018508/1) and the University of Exeter (PhD studentship for Teuntje P. Hollaar). The International Continental Scientific Drilling Program (ICDP) funded the JET project in which this contribution sits.

*Review statement.* This paper was edited by David McLagan and reviewed by Patrick Bartlein and two anonymous referees.

## References

Adie, H., Richert, S., Kirkman, K. P., and Lawes, M. J.: The heat is on: frequent high intensity fire in bracken (Pteridium aquilinum) drives mortality of the sprouting tree Protea caffra in temperate grasslands, Plant Ecol., 212, 2013–2022, https://doi.org/10.1007/s11258-011-9945-8, 2011.

Archibald, S., Roy, D. P., van Wilgen, B. W., and Scholes, R. J.: What limits fire? An examination of drivers of burnt area in Southern Africa, Glob. Change Biol., 15, 613–630, https://doi.org/10.1111/j.1365-2486.2008.01754.x, 2009.

Archibald, S., Lehmann, C. E., Gómez-Dans, J. L., and Bradstock, R. A.: Defining pyromes and global syndromes of fire regimes, P. Natl. Acad. Sci. USA, 110, 6442–6447, https://doi.org/10.1073/pnas.1211466110, 2013.

Archibald, S., Lehmann, C. E., Belcher, C. M., Bond, W. J., Bradstock, R. A., Daniau, A. L., Dexter, K. G., Forreste, E. J., Greve, M., He, T., Higgins, S. I., Hoffmann, W. A., Lamont, B. B., McGlinn, D. J., Moncrieff, G. R., Osborne, C. P., Pausas, J. G., Price, O., Ripley, B. S., Rogers, B. M., Schwilk, D. W., Simon, M. F., Turetsky, M. R., Van der Werf, G. R., and Zanne, A. E.: Biological and geophysical feedbacks with fire in the Earth system, Environ. Res. Lett., 13, 033003, https://doi.org/10.1088/1748-9326/aa9ead, 2018.

Beerling, D. J. and Royer, D. L.: Fossil plants as indicators of the Phanerozoic global carbon cycle, Annu. Rev. Earth Pl. Sc., 30, 527–556, https://doi.org/10.1146/annurev.earth.30.091201.141413, 2002.

Belcher, C. M. and Hudspith, V. A.: Changes to Cretaceous surface fire behaviour influenced the spread of the early angiosperms, New Phytol., 213, 1521–1532, https://doi.org/10.1111/nph.14264, 2017.

Belcher, C. M., Collinson, M. E., and Scott, A. C.: Constraints on the thermal energy released from the Chicxulub impactor: new evidence from multi-method charcoal analysis, J. Geol. Soc. London, 162, 591–602, https://doi.org/10.1144/0016-764904-104, 2005.

Belcher, C. M., Collinson, M. E., and Scott, A. C.: A 450-Million-Year History of Fire, in: Fire Phenomena and the Earth System: An Interdisciplinary Guide to Fire Science, edited by: Belcher, C. M., Wiley, London, UK, https://doi.org/10.1002/9781118529539, 240–241, 2013.

Berger, A., Loutre, M. F., and Dehant, V.: Astronomical frequencies for pre-Quaternary palaeoclimate studies, Terra Nova, 1, 474–479, https://doi.org/10.1111/j.1365-3121.1989.tb00413.x, 1989.

Berner, R. A.: GEOCARBSULF: a combined model for Phanerozoic atmospheric $O_2$ and $CO_2$, Geochim. Cosmochim. Ac., 70, 5653–5664, https://doi.org/10.1016/j.gca.2005.11.032, 2006.

Bonis, N. R., Ruhl, M., and Kürschner, W. M.: Milankovitch-scale palynological turnover across the Triassic–Jurassic transition at St. Audrie's Bay, SW UK, J. Geol. Soc. London, 167, 877–888, https://doi.org/10.1144/0016-76492009-141, 2010.

Bos, R., Lindström, S., van Konijnenburg-van Cittert, H., Hilgen, F., Hollaar, T. P., Aalpoel, H., van der Weijst, C., Sanei, H., Rudra, A., Sluijs, A., and van de Schootbrugge, B.: Triassic-Jurassic vegetation response to carbon cycle perturbations and climate change, Global Planet. Change, 228, 104211, https://doi.org/10.1016/j.gloplacha.2023.104211, 2023.

Bougeault, C., Pellenard, P., Deconinck, J. F., Hesselbo, S. P., Dommergues, J. L., Bruneau, L., Cocquerez, T., Laffont,

R., Huret, E., and Thibault, N.: Climatic and palaeoceanographic changes during the Pliensbachian (Early Jurassic) inferred from clay mineralogy and stable isotope (CO) geochemistry (NW Europe), Global Planet. Change, 149, 139–152, https://doi.org/10.1016/j.gloplacha.2017.01.005, 2017.

Bowman, D. M., Murphy, B. P., Williamson, G. J., and Cochrane, M. A.: Pyrogeographic models, feedbacks and the future of global fire regimes, Global Ecol. Biogeogr., 23, 821–824, https://doi.org/10.1111/geb.12180, 2014.

Bradstock, R. A.: A biogeographic model of fire regimes in Australia: current and future implications, Global Ecol. Biogeogr., 19, 145–158, https://doi.org/10.1111/j.1466-8238.2009.00512.x, 2010.

Brown, S. A., Scott, A. C., Glasspool, I. J., and Collinson, M. E.: Cretaceous wildfires and their impact on the Earth system, Cretaceous Res., 36, 162–190, https://doi.org/10.1016/j.cretres.2012.02.008, 2012.

Chamley, H.: Clay Sedimentology, Springer Berlin Heidelberg, Heidelberg, https://doi.org/10.1007/978-3-642-85916-8, 1989.

Cochrane, M. A.: Fire science for rainforests, Nature, 421, 913–919, https://doi.org/10.1038/nature01437, 2003.

Cochrane, M. A. and Ryan, K. C.: Fire and fire ecology: Concepts and principles, in: Tropical Fire Ecology, Springer, 25–62, https://doi.org/10.1007/978-3-540-77381-8_2, 2009.

Collinson, M. E., Featherstone, C. Cripps, J.A, Nichols, G. J., and Scott, A. C.: Charcoal-rich plant debris accumulations in the Lower Cretaceous of the Isle of Wight, England, Acta Palaeobotanica, 2, 93–105, 2000.

Collinson, M. E., Steart, D. C., Scob, A. C., Glasspool, I. J., and Hooker, J. J.: Episodic fire, runoff and deposition at the Palaeocene–Eocene boundary, J. Geol. Soc., 164, 87–97, https://doi.org/10.1144/0016-76492005-185, 2007.

Collinson, M. E., Steart, D. C., Harrington, G. J., Hooker, J. J., Scob, A. C., Allen, L. O., Glasspool, I. J., and Gibbons, S. J.: Palynological evidence of vegetation dynamics in response to palaeoenvironmental change across the onset of the Paleocene-Eocene Thermal Maximum at Cobham, Southern England, Grana, 48, 38–66, https://doi.org/10.1080/00173130802707980, 2009.

Daniau, A. L., Sánchez-Goñi, M. F., Beaufort, L., Laggoun-Défarge, F., Loutre, M. F., and Duprat, J.: Dansgaard–Oeschger climatic variability revealed by fire emissions in southwestern Iberia, Quaternary Sci. Rev., 26, 1369–1383, https://doi.org/10.1016/j.quascirev.2007.02.005, 2007.

Daniau, A. L., Bartlein, P. J., Harrison, S. P., Prentice, I. C., Brewer, S., Friedlingstein, P., Harrison-Prentice, T. I., Inoue, J., Izumi, K., Marlon, J. R., Mooney, S., Power, M. J., Stevenson, J., Tinner, W., Andrič, M., Atanassova, J., Behling, H., Black, M., Blarquez, O., Brown, K. J., Carcaillet, C., Colhoun, E. A., Colombaroli, D., Davis, B. A. S., D'Costa, D., Dodson, J., Dupont, L., Eshetu, Z., Gavin, D. G., Genries, A., Haberle, S., Hallett, D. J., Hope, G., Horn, S. P., Kassa, T. G., Katamura, F., Kennedy, L. M., Kershaw, P., Krivonogov, S., Long, C., Magri, D., Marinova, E., McKenzie, G. M., Moreno, P. I., Moss, P., Neumann, F. H., Norström, E., Paitre, C., Rius, D., Roberts, N., Robinson, G. S., Sasaki, N., Scott, L., Takahara, H., Terwilliger, V., Thevenon, F., Turner, R., Valsecchi, V. G., Vannière, B., Walsh, M., Williams, N., and Zhang, Y.: Predictability of biomass burning in response to climate changes, Global Biogeochem. Cy., 26, https://doi.org/10.1029/2011GB004249, 2012.

Danisch, J., Kabiri, L., Nutz, A., and Bodin, S.: Chemostratigraphy of late Sinemurian–early Pliensbachian shallow-to deep-water deposits of the Central High Atlas Basin: Paleoenvironmental implications, J. Afr. Earth Sci., 153, 239–249, https://doi.org/10.1016/j.jafrearsci.2019.03.003, 2019.

De Graciansky, P. C., Dardeau, G., Dommergues, J. L., Durlet, C., Marchand, D., Dumont, T., Hesselbo, S. P., Jacquin, T., Marchand, D., Meister, C., Mouterde, R., Rey, J., and Vail, P. R.: Ammonite biostratigraphic correlation and Early Jurassic sequence stratigraphy in France: comparisons with some UK sections, in: Mesozoic and Cenozoic Sequence Statigraphy of European Basins, edited by: de Graciansky, P. C., Hardenbol, J., Jacquin, T., Farley, M., and Vail, P. R., SEPM Spec. P., 60, 583–622, 1998.

Deconinck, J. F., Hesselbo, S. P., and Pellenard, P.: Climatic and sea-level control of Jurassic (Pliensbachian) clay mineral sedimentation in the Cardigan Bay Basin, Llanbedr (Mochras Farm) borehole, Wales, Sedimentology, 66, 2769–2783, https://doi.org/10.1111/sed.12610, 2019.

Glasspool, I. J. and Gastaldo, R. A.: Silurian wildfire proxies and atmospheric oxygen, Geology, 50, 1048–1052, https://doi.org/10.1130/G50193.1, 2022.

Glasspool, I. J., Edwards, D., and Axe, L.: Charcoal in the Silurian as evidence for the earliest wildfire, Geology, 32, 381–383, https://doi.org/10.1130/G20363.1, 2004.

Gómez, J. J., Comas-Rengifo, M. J., and Goy, A.: Palaeoclimatic oscillations in the Pliensbachian (Early Jurassic) of the Asturian Basin (Northern Spain), Clim. Past, 12, 1199–1214, https://doi.org/10.5194/cp-12-1199-2016, 2016.

Hammer, Ø., Harper, D. A. T., and Ryan, P. D.: PAST: Paleontological statistics software package for education and data analysis, Palaeontol. Electron., 4, 9 pp., http://palaeo-electronica.org/2001_1/past/issue1_01.htm (last access: 17 May 2024), 2001.

Haq, B. U.: Jurassic sea-level variations: a reappraisal, GSA Today, 28, 4–10, https://doi.org/10.1130/GSATG359A.1, 2018.

Harris, T. M.: Burnt ferns from the English Wealden, P. Geologist. Assoc., 92, 47–58, https://doi.org/10.1016/S0016-7878(81)80019-3, 1981.

Hesselbo, S. P. and Jenkyns, H. C.: British Lower Jurassic sequence stratigraphy, in: Mesozoic–Cenozoic Sequence Stratigraphy of European Basins, edited by: de Graciansky, P. C., Hardenbol, J., Jacquin, T., Farley, M., and Vail, P. R., SEPM Spec. P., 60, 561–581, 1998.

Hinnov, L. A., Ruhl, M. R., and Hesselbo, S. P.: Reply to the Comment on "Astronomical constraints on the duration of the Early Jurassic Pliensbachian Stage and global climatic fluctuations" (Ruhl et al., (2016), Earth Planet. Sc. Lett., 455, 149–165), 481, 415–419, https://doi.org/10.1016/j.epsl.2017.10.061, 2018.

Hollaar, T. P.: Terrestrial palaeo-environmental proxy data of the Upper Pliensbachian, Mochras Borehole sediments, deposited in the Cardigan Bay Basin, Wales, NERC EDS National Geoscience Data Centre [data set], https://doi.org/10.5285/d6b7c567-49f0-44c7-a94c-e82fa17ff98e, 2021.

Hollaar, T. P.: Palynofacies, microcharcoal, clay mineralogical and carbon isotope mass spectrometry measurements from the Late Pliensbachian (934–918 mbs) of the Mochras core, Cardigan Bay Basin, NW Wales, UK, NERC EDS National Geoscience Data Centre [data set], https://doi.org/10.5285/1461dbe5-50a8-425c-8c49-ac1f04bcc271, 2022.

Hollaar, T. P.: Data from the Sinemurian-Pliensbachian boundary charcoal, clay, C-isotopes and palynofacies, Mochras core, NW Wales, UK, NERC EDS National Geoscience Data Centre [data set], https://doi.org/10.5285/2ec864e0-cb08-44c0-92fe-07af2ef93e3a, 2024.

Hollaar, T. P., Baker, S. J., Hesselbo, S. P., Deconinck, J. F., Mander, L., Ruhl, M., and Belcher, C. M.: Wildfire activity enhanced during phases of maximum orbital eccentricity and precessional forcing in the Early Jurassic, Communications Earth and Environment, 2, 1–12, https://doi.org/10.1038/s43247-021-00307-3, 2021.

Hollaar, T. P., Hesselbo, S. P., Deconinck, J.-F., Damaschke, M., Ullmann, C. V., Jiang, M., and Belcher, C. M.: Environmental changes during the onset of the Late Pliensbachian Event (Early Jurassic) in the Cardigan Bay Basin, Wales, Clim. Past, 19, 979–997, https://doi.org/10.5194/cp-19-979-2023, 2023.

Imbrie, J. and Imbrie, J. Z.: Modeling the climatic response to orbital variations, Science, 207, 943–953, https://doi.org/10.1126/science.207.4434.943, 1980.

Korte, C. and Hesselbo, S. P.: Shallow marine carbon and oxygen isotope and elemental records indicate icehouse-greenhouse cycles during the Early Jurassic, Paleoceanography, 26, PA4219, https://doi.org/10.1029/2011PA002160, 2011.

Korte, C., Hesselbo, S. P., Ullmann, C. V., Dietl, G., Ruhl, M., Schweigert, G., and Thibault, N.: Jurassic climate mode governed by ocean gateway, Nat. Commun., 6, 1–7, https://doi.org/10.1038/ncomms10015, 2015.

Krawchuk, M. A. and Moritz, M. A.: Constraints on global fire activity vary across a resource gradient, Ecology, 92, 121–132, https://doi.org/10.1890/09-1843.1, 2011.

Legarreta, L. and Uliana, M. A.: The Jurassic succession in west-central Argentina: stratal patterns, sequences and paleogeographic evolution, Palaeogeogr. Palaeocl., 120, 303–330, https://doi.org/10.1016/0031-0182(95)00042-9, 1996.

Li, X., Wang, J., Rasbury, T., Zhou, M., Wei, Z., and Zhang, C.: Early Jurassic climate and atmospheric $CO_2$ concentration in the Sichuan paleobasin, southwestern China, Clim. Past, 16, 2055–2074, https://doi.org/10.5194/cp-16-2055-2020, 2020.

Martinez, M. and Dera, G.: Orbital pacing of carbon fluxes by a ∼9-My eccentricity cycle during the Mesozoic, P. Natl. Acad. Sci. USA, 112, 12604–12609, https://doi.org/10.1073/pnas.1419946112, 2015.

McElwain, J. C., Wade-Murphy, J., and Hesselbo, S. P.: Changes in carbon dioxide during an oceanic anoxic event linked to intrusion into Gondwana coals, Nature, 435, 479–482, https://doi.org/10.1038/nature03618, 2005.

Meyn, A., White, P. S., Buhk, C., and Jentsch, A.: Environmental drivers of large, infrequent wildfires: the emerging conceptual model, Prog. Phys. Geog., 31, 287–312, https://doi.org/10.1177/0309133307079365, 2007.

Moore, D. M. and Reynolds Jr., R. C.: X-ray Diffraction and the Identification and Analysis of Clay Minerals, Oxford University Press, Oxford, ISBN: 9780195087130, 1997.

Munier, T., Deconinck, J.-F., Pellenard, P., Hesselbo, S. P., Riding, J. B., Ullmann, C. V., Bougeault, C., Mercuzot, M., Santoni, A.-L., Huret, É., and Landrein, P.: Million-year-scale alternation of warm–humid and semi-arid periods as a mid-latitude climate mode in the Early Jurassic (late Sinemurian, Laurasian Seaway), Clim. Past, 17, 1547–1566, https://doi.org/10.5194/cp-17-1547-2021, 2021.

Nichols, G. J., Cripps, J. A., Collinson, M. E., and Scott, A. C.: Experiments in waterlogging and sedimentology of charcoal: results and implications, Palaeogeogr. Palaeocl., 164, 43–56, https://doi.org/10.1016/S0031-0182(00)00174-7, 2000.

Oboh-Ikuenobe, F. E., Obi, C. G., and Jaramillo, C. A.: Lithofacies, palynofacies, and sequence stratigraphy of Palaeogene strata in Southeastern Nigeria, J. Afr. Earth Sci., 41, 79–101, https://doi.org/10.1016/j.jafrearsci.2005.02.002, 2005.

Pausas, J. G. and Bradstock, R. A.: Fire persistence traits of plants along a productivity and disturbance gradient in mediterranean shrublands of south-east Australia, Global Ecol. Biogeogr., 16, 330–340, https://doi.org/10.1111/j.1466-8238.2006.00283.x, 2007.

Pausas, J. G. and Paula, S.: Fuel shapes the fire–climate relationship: evidence from Mediterranean ecosystems, Global Ecol. Biogeogr., 21, 1074–1082, https://doi.org/10.1111/j.1466-8238.2012.00769.x, 2012.

Pausas, J. G. and Ribeiro, E.: The global fire–productivity relationship, Global Ecol. Biogeogr., 22, 728–736, https://doi.org/10.1111/geb.12043, 2013.

Petschick, R.: MacDiff 4.1.2. Powder diffraction software, https://www.uni-frankfurt.de/69620898/Petschick_MacDiff (last access: 17 May 2024), 2000.

Pieńkowski, G., Uchman, A., Ninard, K., and Hesselbo, S. P.: Ichnology, sedimentology, and orbital cycles in the hemipelagic Early Jurassic Laurasian Seaway (Pliensbachian, Cardigan Bay Basin, UK), Global Planet. Change, 207, 103648, https://doi.org/10.1016/j.gloplacha.2021.103648, 2021.

Rees, P. M., Ziegler, A. M., and Valdes, P. J.: Jurassic phytogeography and climates: new data and model comparisons, in: Warm Climates in Earth History, edited by: Huber, B. T., Macleod, K. G., and Wing, S. L., Cambridge University Press, Cambridge, ISBN: 0 521 64142 X, 297–318, 2000.

Retallack, G. J.: A 300-million-year record of atmospheric carbon dioxide from fossil plant cuticles, Nature, 411, 287–290, https://doi.org/10.1038/35077041, 2001.

Riding, J. B., Leng, M. J., Kender, S., Hesselbo, S. P., and Feist-Burkhardt, S.: Isotopic and palynological evidence for a new Early Jurassic environmental perturbation, Palaeogeogr. Palaeocl., 374, 16–27, https://doi.org/10.1016/j.palaeo.2012.10.019, 2013.

Robinson, S. A., Ruhl, M., Astley, D. L., Naafs, B. D. A., Farnsworth, A. J., Bown, P. R., Jenkyns, H. C., Lunt, D. J., O'Brien, C., Pancost, R. D., and Markwick, P. J.: Early Jurassic North Atlantic sea-surface temperatures from TEX86 palaeothermometry, Sedimentology, 64, 215–230, https://doi.org/10.1111/sed.12321, 2017.

Rubincam, D. P.: Insolation in terms of Earth's orbital parameters, Theor. Appl. Climatol., 48, 195–202, https://doi.org/10.1007/BF00867049, 1994.

Ruffell, A., McKinley, J. M., and Worden, R. H.: Comparison of clay mineral stratigraphy to other proxy palaeoclimate indicators in the Mesozoic of NW Europe, Philos. T. R. Soc. A., 360, 675–693, https://doi.org/10.1098/rsta.2001.0961, 2002.

Ruhl, M., Hesselbo, S. P., Hinnov, L., Jenkyns, H. C., Xu, W., Riding, J. B., Minisini, D., Ullmann, C. V., and Leng, M. J.: Astronomical constraints on the duration of the Early Jurassic Pliens-

bachian Stage and global climatic fluctuations, Earth Planet. Sc. Lett., 455, 149–165, https://doi.org/10.1016/j.epsl.2016.08.038, 2016.

Scott, A. C.: The Pre-Quaternary history of fire, Palaeogeogr. Palaeocl., 164, 281–329, https://doi.org/10.1016/S0031-0182(00)00192-9, 2000.

Scott, A. C. and Damblon, F.: Charcoal: Taphonomy and significance in geology, botany and archaeology, Palaeogeogr. Palaeocl., 291, 1–10, https://doi.org/10.1016/j.palaeo.2010.03.044, 2010.

Sellwood, B. W. and Valdes, P. J.: Jurassic climates, P. Geologist Assoc., 119, 5–17, https://doi.org/10.1016/S0016-7878(59)80068-7, 2008.

Silva, R. L., Duarte, L. V., Wach, G. D., Ruhl, M., Sadki, D., Gómez, J. J., Hesselbo, S.P., Xu, W., O'Connor, D., Rodrigues, B., and Mendonça Filho, J. G.: An Early Jurassic (Sinemurian–Toarcian) stratigraphic framework for the occurrence of organic matter preservation intervals (OMPIs), Earth-Sci. Rev., 221, 103780, https://doi.org/10.1016/j.earscirev.2021.103780, 2021.

Slater, S. M., Twitchett, R. J., Danise, S., and Vajda, V.: Substantial vegetation response to Early Jurassic global warming with impacts on oceanic anoxia, Nat. Geosci., 12, 462–467, https://doi.org/10.1038/s41561-019-0349-z, 2019.

Steinthorsdottir, M. and Vajda, V.: Early Jurassic (late Pliensbachian) $CO_2$ concentrations based on stomatal analysis of fossil conifer leaves from eastern Australia, Gondwana Res., 27, 932–939, https://doi.org/10.1016/j.gr.2013.08.021, 2015.

Storm, M. S., Hesselbo, S. P., Jenkyns, H. C., Ruhl, M., Ullmann, C. V., Xu, W., Leng, M. J., Riding, J. B., and Gorbanenko, O.: Orbital pacing and secular evolution of the Early Jurassic carbon cycle, P. Natl. Acad. Sci. USA, 117, 3974–3982, https://doi.org/10.1073/pnas.1912094117, 2020.

The MathWorks Inc.: MATLAB version: 9.11.0 (R2021b), The MathWorks Inc., Natick, Massachusetts, https://www.mathworks.com (last access: 17 May 2024), 2021.

The MathWorks Inc.: MATLAB version: 9.14.0 (R2023b), The MathWorks Inc., Natick, Massachusetts, https://www.mathworks.com (last access: 17 May 2024), 2023.

Torsvig, T. H. and Cox, L. R. M: Earth History and Palaeogeography Cambridge University Press, 316 pp., ISBN-13: 978-1107105324, 2017.

Trenberth, K. E., Fasullo, J., and Smith, L.: Trends and variability in column-integrated atmospheric water vapor, Clim. Dynam., 24, 741–758, https://doi.org/10.1007/s00382-005-0017-4, 2005.

Ullmann, C. V., Szűcs, D., Jiang, M., Hudson, A. J., and Hesselbo, S. P.: Geochemistry of macrofossil, bulk rock and secondary calcite in the Early Jurassic strata of the Llanbedr (Mochras Farm) drill core, Cardigan Bay Basin, Wales, UK, J. Geol. Soc. London, 179, jgs2021-018, https://doi.org/10.1144/jgs2021-018, 2022.

van de Schootbrugge, B., Bailey, T. R., Rosenthal, Y., Katz, M. E., Wright, J. D., Miller, K. G., Feist-Burkhardt, S., and Falkowski, P. G.: Early Jurassic climate change and the radiation of organic-walled phytoplankton in the Tethys Ocean, Paleobiology, 31, 73–97, https://doi.org/10.1666/0094-8373(2005)031<0073:EJCCAT>2.0.CO;2, 2005.

van der Werf, G. R., Randerson, J. T., Giglio, L., Collatz, G. J., Kasibhatla, P. S., and Arellano Jr., A. F.: Interannual variability in global biomass burning emissions from 1997 to 2004, Atmos. Chem. Phys., 6, 3423–3441, https://doi.org/10.5194/acp-6-3423-2006, 2006.

Van Konijnenburg-Van Cibert, J. H. A.: Ecology of some late Triassic to early Cretaceous ferns in Eurasia, Rev. Palaeobot. Palyno., 119, 113–124, https://doi.org/10.1016/S0034-6667(01)00132-4, 2002.

Westerhold, T., Marwan, N., Drury, A. J., Liebrand, D., Agnini, C., Anagnostou, E., Barnet, J. S. K., Bohaty, S. M., De Vleeschouwer, D., Florindo, F., Frederichs, T., Hodell, D. A., Holbourn, A. E., Kroon, D., Lauretano, V., Littler K., Lourens L. J., Lyle, M., Pälike, H., Röhl, U., Tian, J., Wilkens, R. H., Wilson, P. A., and Zachos J. C.: An astronomically dated record of Earth's climate and its predictability over the last 66 million years, Science, 369, 1383–1387, https://doi.org/10.1126/science.aba6853, 2020.

Willis, K. J. and McElwain, J. C.: The Evolution of Plants, 2nd Edition, Oxford University Press, 408 pp., ISBN: 9780199292233, 2013.

Woodward, C. and Haines, H. A.: Unprecedented long-distance transport of macroscopic charcoal from a large, intense forest fire in eastern Australia: implications for fire history reconstruction, Holocene, 30, 947–952, https://doi.org/10.1177/0959683620908664, 2020.

Xu, W., Ruhl, M., Jenkyns, H. C., Leng, M. J., Huggett, J. M., Minisini, J. M., Ullmann, C. V., Riding, J. B., Weijers, J. W. H., Storm, M. S., and Hesselbo, S. P.: Evolution of the Toarcian (Early Jurassic) carbon-cycle and global climatic controls on local sedimentary processes (Cardigan Bay Basin, UK), Earth Planet. Sc. Lett., 484, 396–411, 2018.